Paulo Cesar Plaisant Junior
EMBRAER
São José dos Campos/SP – Brazil
paulo.plaisant@embraer.com.br

Flávio Luiz de Silva Bussamra*
Instituto Tecnológico de Aeronáutica
São José dos Campos/SP – Brazil
flaviobu@ita.br

Francisco Kioshi Arakaki
EMBRAER
São José dos Campos/SP – Brazil
francisco.arakaki@embraer.com.br

*author for correspondence

Finite element procedure for stress amplification factor recovering in a representative volume of composite materials

Abstract: *Finite element models are proposed to the micromechanical analysis of a representative volume of composite materials. A detailed description of the meshes, boundary conditions, and loadings are presented. An illustrative application is given to evaluate stress amplification factors within a representative volume of the unidirectional carbon fiber composite plate. The results are discussed and compared to the numerical findings.*
Keywords: *Micromechanics, Finite element analysis, Composites, Stress amplification factor, Microstress distribution.*

INTRODUCTION

By analyzing history, it is possible to see the importance of material science applied to Aeronautical Engineering and, in that scenario, the composite materials emerged. As this type of material became more recognized, new branches of research came out. One of these branches is the micromechanics, which is the theory that this study focuses on. Since composite materials play an important role in the modern industry, it is necessary a better understanding of them. Particularly in aeronautical industry, metal alloys have been replaced by composite materials. The best example is the latest Boeing aircraft, 787: 50% of its structure is made of composite materials and 20% of aluminum. Its predecessor has 12% of composite materials and 50% of aluminum (Boeing, 2010).

The analysis of composite materials follows a macro, meso, or micromechanical approach. Macromechanics analyzes a laminated plate as a homogeneous anisotropic equivalent plate. In the mesomechanical approach, a laminate is modeled as a stacking sequence of homogeneous layers and interlaminar interfaces (Ladevèze *et al.*, 2005), therefore the prediction of complex behavior, as delamination, can be assessed (Allix, Ladevèze and Corigliano, 1995). The micromechanical analysis goes down to the constituent properties. The object of study on the micromechanical analysis is the representative volume element (RVE), or unit cell, which is the smallest cell capable of representing the overall response of the unidirectional ply to mechanical and thermal loading (Jin *et al.*, 2008). Figure 1 illustrates an example of RVE.
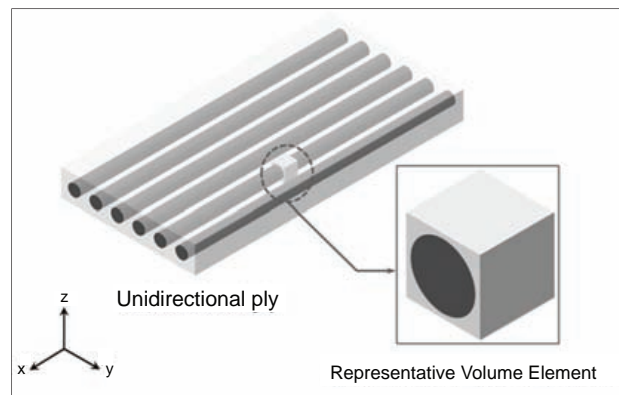
Figure 1. Representative volume element in a unidirectional fiber composite ply.

Jin *et al.* (2008) show the use of three-dimensional finite element models for obtaining stress distribution on composites. Micromechanical finite element models provide data to obtain the micro-stresses at the matrix/fiber interface, and great benefits can be reached when a micromechanical approach is considered. Micromechanics of failure gives a more precise way of composite failure prediction. With the micro-stresses, it is possible to determine the failure initiation in the unidirectional ply (Ha, Huang and Jin, 2008a; Tay *et al.*, 2008; Gotsis, Chamis and Minnetyan, 1998). The material lifetime forecast can be obtained with the use of micromechanics of failure associated with the Accelerated Testing Method (ATM) and Evolution of Damage (Sihn and Park, 2008; Ha, Huang and Jin, 2008b).

The micromechanical theory considers not only the mechanical loads, but also environmental factors, such as thermal loads, as a result of temperature variation and moisture (Hyer and Waas, 2000; Fiedler, Hojo and Ochiai, 2002).

The influence of fiber arrangements on mechanical behavior of laminated pates is discussed by Hojo *et al.* (2009) and Ha, Huang and Jin (2008c). Considerations about the fabrication process are discussed by Aghdam and Khojeh (2003). Studies with reinforcements other than fibers, such as particles, are exposed by Zhu, Cai and Tu (2009). Different types of composites, like bulk metallic glasses (Dragoi *et al.*, 2001), metallic matrix composites (Chaboche, Kruch and Pottier, 1998), and smart composites, which include piezoelectric composites, shape memory alloy (SMA) fiber composites, and piezoresistive composites (Taya, 1999), are also analyzed by micromechanics. Liang, Lee and Suaris (2006) present the results of a comparison between micromechanical finite elements modeling and mechanical testing. RVE use in order to represent the composite material is discussed by Sun e Vaidya (1995), and a study of boundary conditions for the unit cell is shown by Xia *et al.* (2003). From the aeronautical industry to dentistry, a great variety of products can be benefited from a micromechanical study of a composite material. Sakaguchi, Wiltbank and Murchison (2003) show micromechanical studies to predict composite elastic modulus and polymerization shrinkage for dental materials.

The micromechanical theory has direct application for the aeronautical industry. Tsai (2008) points out the use of micromechanics to:

- predict macro mechanical properties (stiffness constants, expansion coefficients);

- control the deformation from mechanical and thermal loads;

- predict a successive ply failure after the first ply failure and;

- adjust empirical data by using micromechanical data.

The objective of this paper is to present and to discuss a methodology in order to obtain the stress amplification factors derived from mechanical and thermal loads in a RVE, with the use of two and three-dimensional finite elements models. Also, this paper aims at accessing stress amplification factors in an orthotropic unidirectional ply with epoxy matrix, carbon fiber, and a perfectly bonded matrix/fiber interface, with 60% of fiber volume fraction. The materials remain in the linear elastic domain. The finite element models are analyzed with the commercial software MSC/NASTRAN, version 70.0.6 (MSC, 2011).

STRESS AMPLIFICATION FACTORS

In a micromechanical level, there is a difference between the applied and actual stresses within the material, mostly because of the dissimilarity on physical properties of the materials. For example, epoxy matrixes present a lower young modulus than the carbon fiber. When a load is applied to a composite material, due to this stiffness difference, the matrix and the fiber tend to show different stresses, resulting in stress concentrations. Therefore, when a unit load is applied to the material, the stresses within the representative volume are no longer unitary, as shown in Fig. 2.
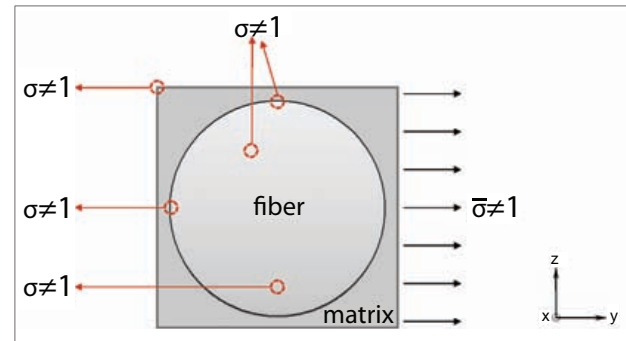

Figure 2. Differences between micro and macro stresses.

Jin *et al.* (2008) show that there are amplification factors which relates a uniformly distributed unit load ($\bar{\sigma}$, the macro mechanical load) and the internal micromechanical stresses σ, expressed in Eq. 1:

$$\sigma = \mathbf{M}\bar{\sigma} + \mathbf{A}\,\Delta T \tag{1}$$

where,

M and A are matrices that collect the mechanical and thermal stress amplification factors, respectively, and ΔT is the increase of the room temperature.

Considering all stress components, referred to the material coordinate system xyz (the same as 123), Eq. 1 can be expanded by Eq. 2 (Jin *et al.*, 2008):

$$\begin{Bmatrix} \sigma_1 = \sigma_{xx} \\ \sigma_2 = \sigma_{yy} \\ \sigma_3 = \sigma_{zz} \\ \sigma_4 = \sigma_{yz} \\ \sigma_5 = \sigma_{zx} \\ \sigma_6 = \sigma_{xy} \end{Bmatrix} = \begin{bmatrix} M_{11} & M_{12} & M_{13} & M_{14} & 0 & 0 \\ M_{21} & M_{22} & M_{23} & M_{24} & 0 & 0 \\ M_{31} & M_{32} & M_{33} & M_{34} & 0 & 0 \\ M_{41} & M_{42} & M_{43} & M_{44} & 0 & 0 \\ 0 & 0 & 0 & 0 & M_{55} & M_{56} \\ 0 & 0 & 0 & 0 & M_{65} & M_{66} \end{bmatrix}_\sigma \begin{Bmatrix} \bar{\sigma}_1 \\ \bar{\sigma}_2 \\ \bar{\sigma}_3 \\ \bar{\sigma}_4 \\ \bar{\sigma}_5 \\ \bar{\sigma}_6 \end{Bmatrix} + \begin{Bmatrix} A_1 \\ A_2 \\ A_3 \\ A_4 \\ A_5 \\ A_6 \end{Bmatrix}_\sigma \Delta T \tag{2}$$

M can be found by applying unidirectional mechanical loads, one at a time. For instance, if a uniformly distributed unit load is applied at x direction, with no thermal load, Eq. 2 simplifies to Eq. 3:

$$
\left\{
\begin{array}{c}
\sigma_1 \\
\sigma_2 \\
\sigma_3 \\
\sigma_4 \\
\sigma_5 \\
\sigma_6
\end{array}
\right\}
=
\left[
\begin{array}{cccccc}
M_{11} & M_{12} & M_{13} & M_{14} & 0 & 0 \\
M_{21} & M_{22} & M_{23} & M_{24} & 0 & 0 \\
M_{31} & M_{32} & M_{33} & M_{34} & 0 & 0 \\
M_{41} & M_{42} & M_{43} & M_{44} & 0 & 0 \\
0 & 0 & 0 & 0 & M_{55} & M_{56} \\
0 & 0 & 0 & 0 & M_{65} & M_{66}
\end{array}
\right]_\sigma
\left\{
\begin{array}{c}
1 \\
0 \\
0 \\
0 \\
0 \\
0
\end{array}
\right\}
\quad (3)
$$

The resolution of the linear system (Eq. 3) yields Eq. 4:

$$
\left\{
\begin{array}{c}
\sigma_1 \\
\sigma_2 \\
\sigma_3 \\
\sigma_4 \\
\sigma_5 \\
\sigma_6
\end{array}
\right\}
=
\left\{
\begin{array}{c}
M_{11} \\
M_{21} \\
M_{31} \\
M_{41} \\
0 \\
0
\end{array}
\right\}
\quad (4)
$$

Therefore, the stress amplification factors M_{11}, M_{21}, M_{31} and M_{41} will be actually the micromechanical stresses σ_1, σ_2, σ_3 and σ_4, respectively. The same procedure can be applied to all directions. Consequently, the methodology consists of the application of uniformly distributed unit loads to the representative volume model. Thus, the resulting stress at a specific direction gives the corresponding stress amplification factor. Since the stresses at the representative volume vary at each point, the stress amplification factor is not constant.

MATERIALS

The RVE of a composite material with 60% of fiber volume fraction, subjected to an uniformly distributed load $\overline{\sigma}_2$, is sh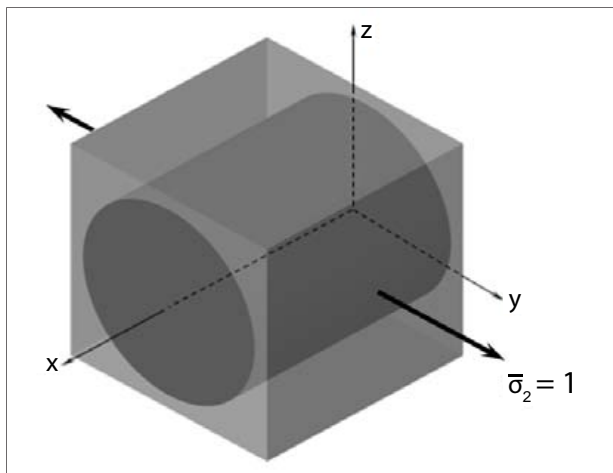owed in Fig. 3. The fiber is represented as a solid cylinder. The mechanical properties of the matrix and fiber are listed in Table 1, where E_{ij} are Young's moduli, ν_{ij} are Poisson's ratios, G_{ij} are shear moduli, and α the thermal expansion coefficient, referred to the material coordinate system xyz (the same as 123).

Table 1. Mechanical properties of the representative volume element materials (Think Composites, 2011).

Carbon fiber		Epoxy matrix	
E_{11} (Pa)	2.35×10^{11}	E_m (Pa)	3.46×10^9
$E_{22}=E_{33}$ (Pa)	1.80×10^{11}	ν_m	0.35
$G_{12}=G_{13}$ (Pa)	7.48×10^9	α_m $(10^{-6}/°C)$	57.6
G_{23} (Pa)	4.90×10^9		
ν_{12}	0.20		
ν_{13}	0.30		
α_1 $(10^{-6}/°C)$	0.0		
α_2, α_3 $(10^{-6}/°C)$	8.3		

NUMERICAL ANALYSIS

Three sets of finite element models are presented and discussed. In the first set, solid hexahedral elements are used to model the matrix and the fiber. The unit cell is represented as a cube with nondimensionalized edge length ($\overline{L} = 1$). Convergence analysis is performed, and stress amplification factors for direct, shear, and thermal loads are presented and discussed. Three-dimensional finite elements are still used in the second set, but the unit cell is no longer modeled as a cube, saving computing efforts. The last set of tests deals with two-dimensional elements. Although they are unable to yield stress concentration factors in transverse directions, in-plane factors are derived. The finite elements solutions are compared with results from Super Mic-Mac software (Think Composites, 2011).

Three-dimensional finite element model

The first set of finite element analysis is applied to a three-dimensional model, with the eight-node hexahedral CHEXA Nastran element for the matrix and fiber modeling. The model, including boundary conditions and loads, are further discussed.

Loads and boundary conditions

When a uniformly distributed tension load is applied to a RVE, the unit cell is constrained at its faces, as shown in Fig. 4, and the free faces must remain flat, as proposed by Jin *et al*. (2008), and Xia, Zhang and Ellyin (2003).

To keep free faces flat, rigid elements are applied to the model. The Nastran rigid element has one master node and one or more slave nodes. The master is the

Figure 3. Representative volume element of a composite material with 60% of fiber volume fraction.

independent one, and it can receive loads. Each slave node will have the same displacements (in the specified direction) of the master one.

Therefore, to keep the right vertical face flat in Fig. 4, a uniformly distributed unit load $\overline{\sigma}_2$ is modeled as a force over only one node. This master node is connected in direction y to the free face nodes (slave nodes) by rigid elements, so all the nodes in this face will have the same displacements in direction y. The nodes in this face must be free at x and z directions (not connected to the master node), in order to move according to the Poisson effect. Rigid body modes are constrained at x=0, y=z=-0.5. Figure 5 shows one model with rigid, spring, and hexahedral elements.
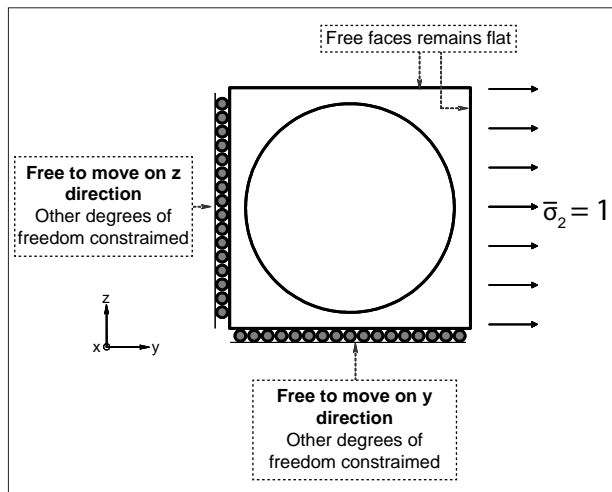

Figure 4. Unit cell constraints, subjected to the uniformly distributed unit load $\overline{\sigma}_2$.
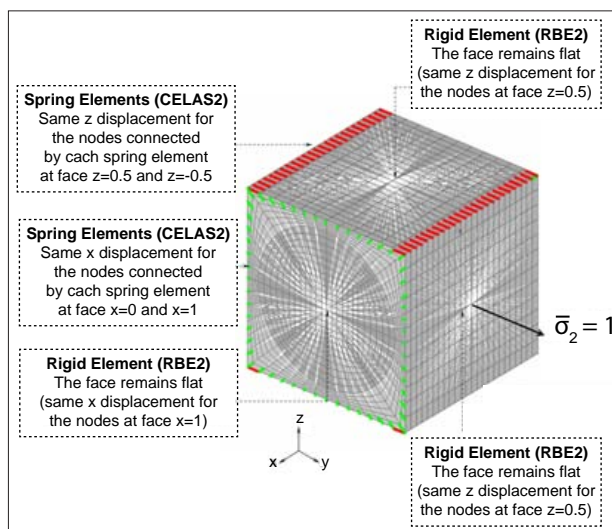

Figure 5. Finite element model with: rigid (RBE2), spring (CELAS2) and hexahedral (CHEXA).

The same procedure must be applied to the others free faces. As it is impossible to enforce two dissimilar displacements on a node, nodes cannot figure as dependent on two different master nodes. Therefore, nodes at the edges are connected by spring elements with high stiffness coefficients. For instance, for face z=0.5 it is necessary to connect the rigid element to the nodes on the edges parallel to the x-axis. However, these nodes are dependent ones on the rigid elements from faces y=0.5 and y=-0.5. Thus, Nastran spring element Celas2, with high stiffness (say, 10^{10}), is used to connect only the z displacements for that particular face and, then, this face remains flat. With the Celas2 element, it is possible to connect only one of the degrees of freedom. From faces z=0.5 and z=-0.5, it is connected the z displacements. For faces x=0 and x=1, it is connected the x displacements.

When a uniformly distributed shear load is applied to the RVE, the unit cell is constrained at its faces as shown in Fig. 6, and proposed by Ha *et al*. (2008). The same procedure already explained is applied here. Rigid body modes are constrained.
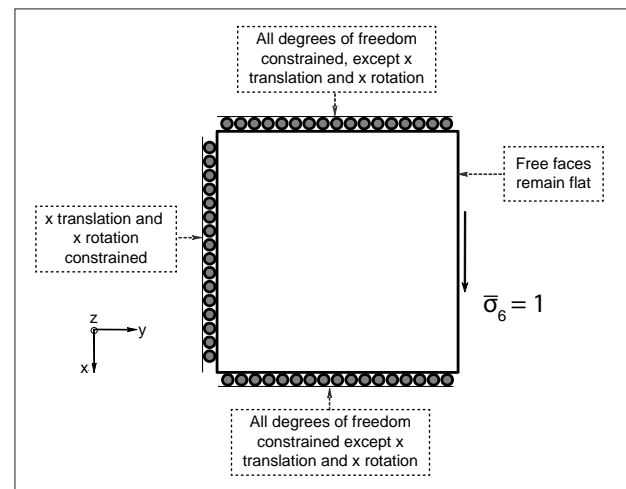

Figure 6. Unit cell constraints, subjected to a uniformly distributed shear load $\overline{\sigma}_6 = 1$.

Convergence analysis

To perform a convergence analysis, a uniformly distributed unit load is applied at direction y. Six finite element meshes are tested (Fig. 7 and Table 2), from a poorly refined 136 element mesh (Mesh 1), to a highly refined 19046 element mesh (Mesh 6).

In order to present the results of the convergence analysis, it is necessary to define a point nomenclature. The points are numbered according to Tay *et al*. (2008), as illustrated in Fig. 8. Points 1, 7 and 4 are the best
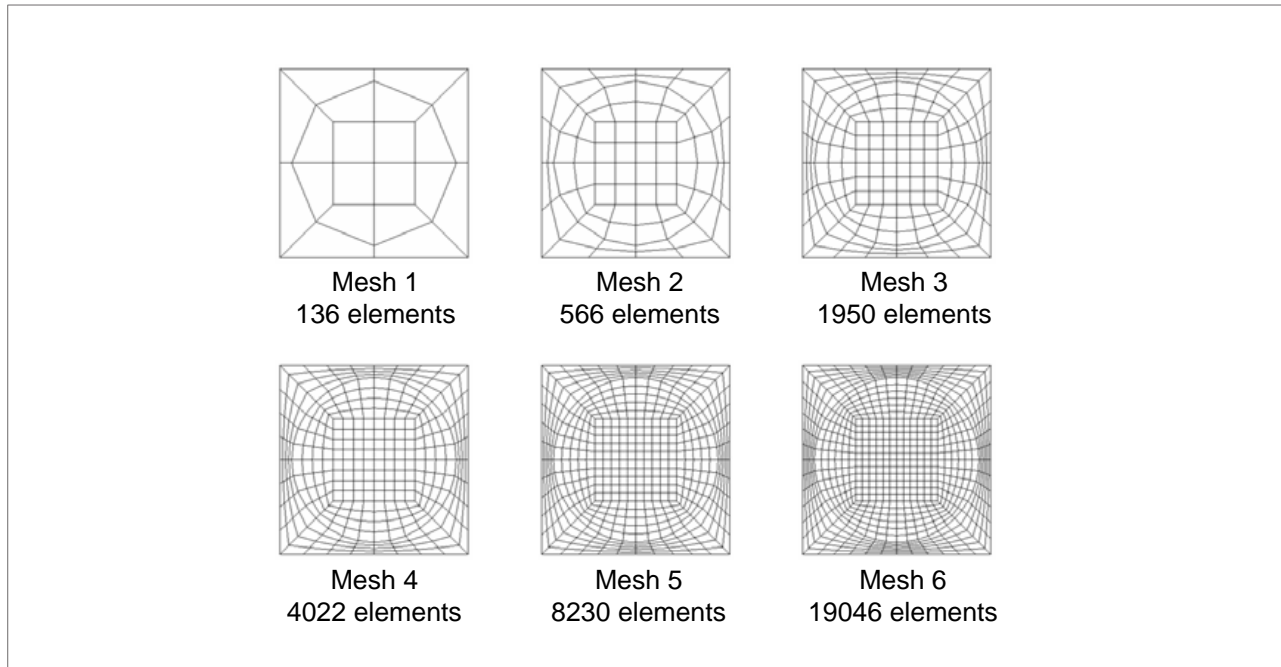
Figure 7. Representative volume three-dimensional element meshes.

Table 2. Number of elements and degree of freedom (DOF) in three-dimensional models.

Mesh	Element type			Total	DOF
	CHEXA	CELAS2	RBE2		
1	80	54	2	136	286
2	480	80	6	566	1641
3	1800	144	6	1950	5813
4	3840	176	6	4022	12171
5	8000	224	6	8230	24999
6	18720	320	6	19046	57765

suitable to have the results displayed, since they are the points of maximum, minimum, and intermediate σ_y stresses, respectively. The results of the convergence testing are shown in Figs. 9 and 10.

It can be seen that after 4,000 elements (Mesh 4), the major stress σ_{max} at Point 1 starts to converge to the value of 1.5. Above 8,000 elements, the results are in the curve asymptotic portion, therefore the chosen mesh is the number 6. Main stresses at points 1, 4 and 7 are compared with results from the Super Mic-Mac Plus (SMM) software (Think Composites, 2011), which are presented in Table 3. SMM has an extensive database of stress amplification factors resultant from finite element analysis for a wide range of physical properties of fiber and matrix, and different volume fractions. It uses interpolation methods to give the values for specifications, which are not in the database.
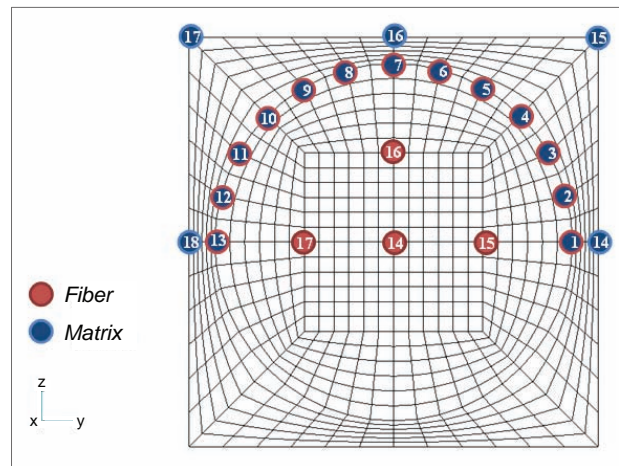

Figure 8. Point nomenclature.

The stress distribution σ_y (micromechanical) at the RVE is shown in Fig. 11. Since the load is $\overline{\sigma}_2 = 1$, the stress distribution σ_y will characterize the stress amplification factor ($M_{22} = 1.55$).

Stress amplification factors for mechanical loads

The stress amplification factors with three-dimensional element meshes are found by applying direct and shear uniformly distributed unit loads at the RVE. As already discussed, the stress contours presented in Figs. 12 and 13 represent the distributions of the stress amplification factors. Table 4 shows all the 36 stress amplification factors at Point 1. These results are compared with solutions by SMM in Tables 5 and 6.
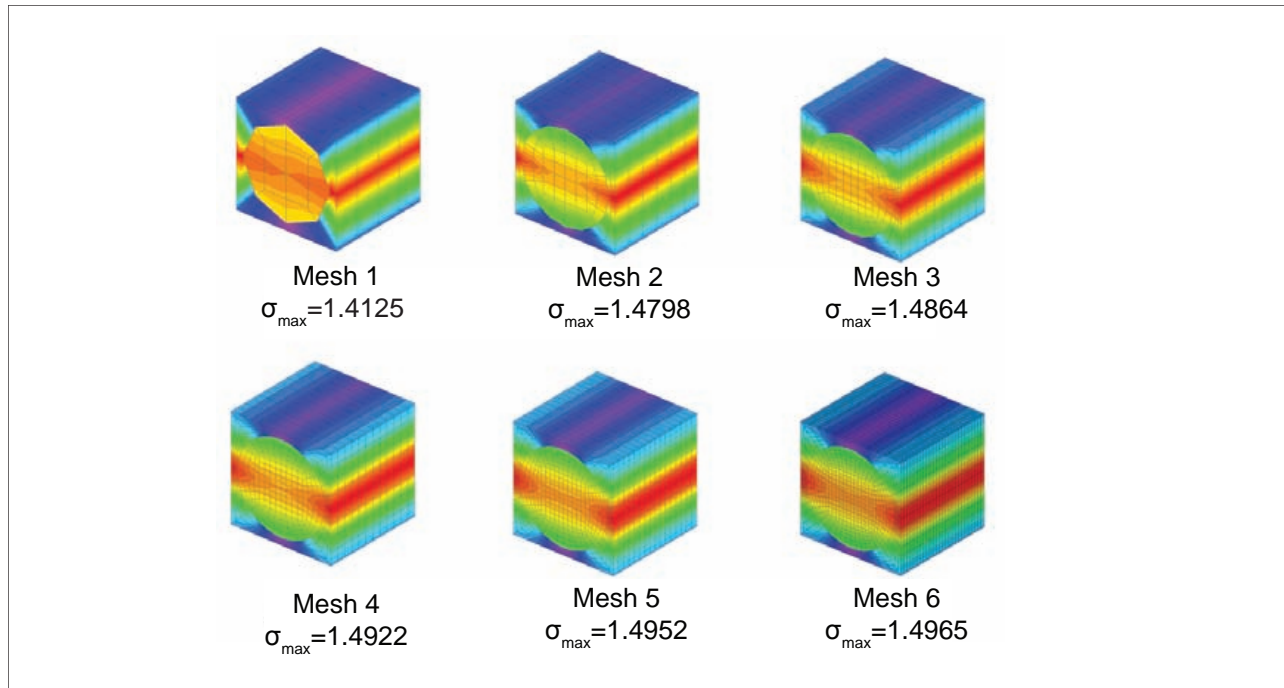
Figure 9. Major stress σ_{max} at the representative volume element.
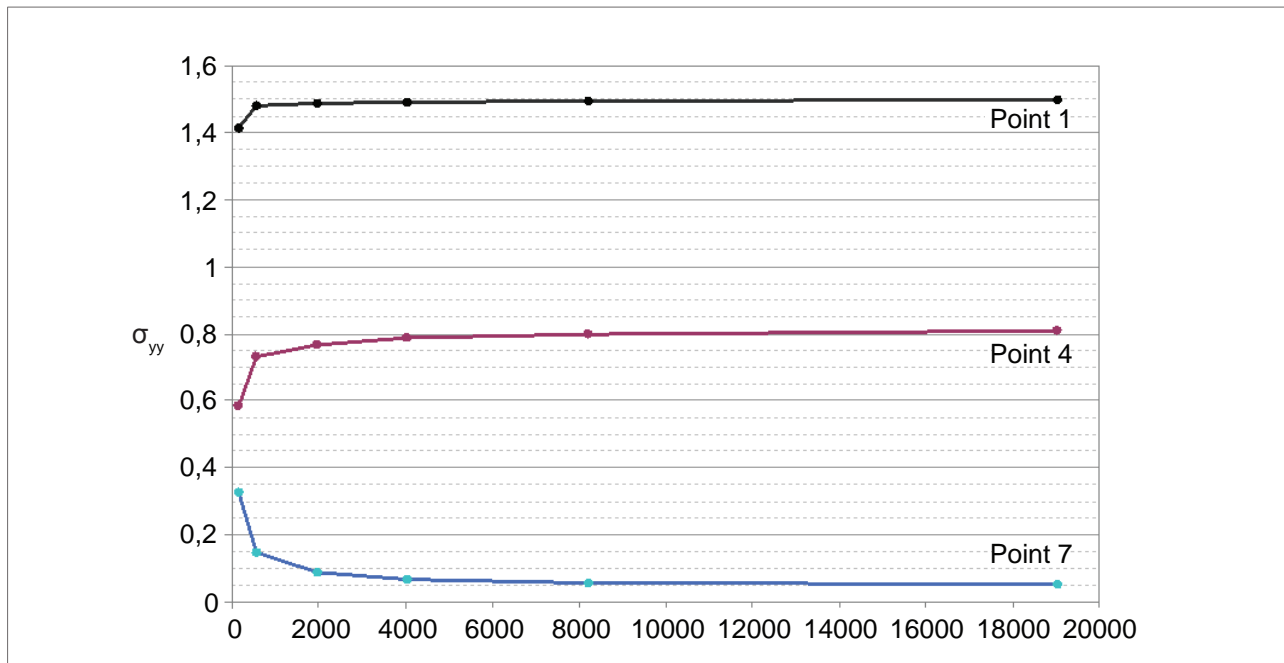
Figure 10. Stress convergence in the representative volume element.

Table 3. Stress recovering for representative volume element subjected to a uniformly distributed load $\overline{\overline{\sigma}}_2 = 1$.

Point	3D model (mesh 6)	SMM	Difference (%)
1	1.49646	1.511233	0.98
4	0.80874	0.810486	0.22
7	0.05139	0.050587	-1.59

Stress amplification factors for thermal loads

Stress amplification factors for thermal loads are obtained by increasing the room temperature by $\Delta T=1^\circ$ C. The finite element analysis with Mesh 6, with the same constraints that were previously discussed, yields the stress contours depicted in Fig. 14. Table 7 presents the differences found with SMM.

Figure 11. Stress amplification factor M_{22}.

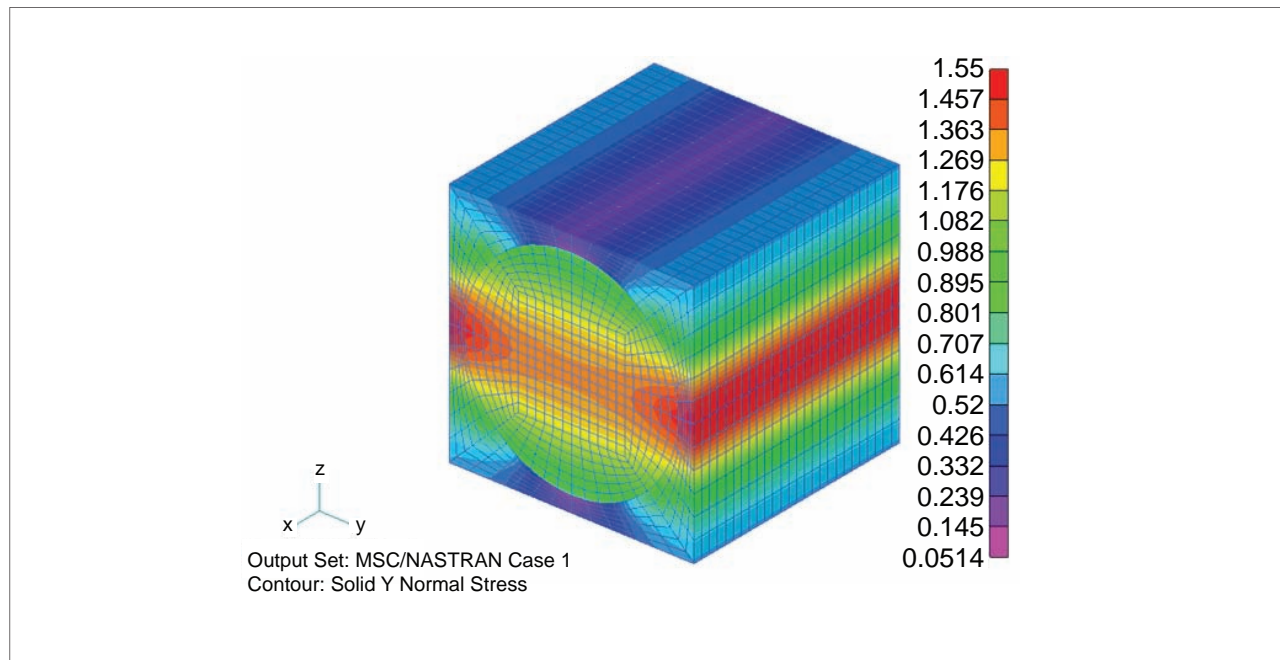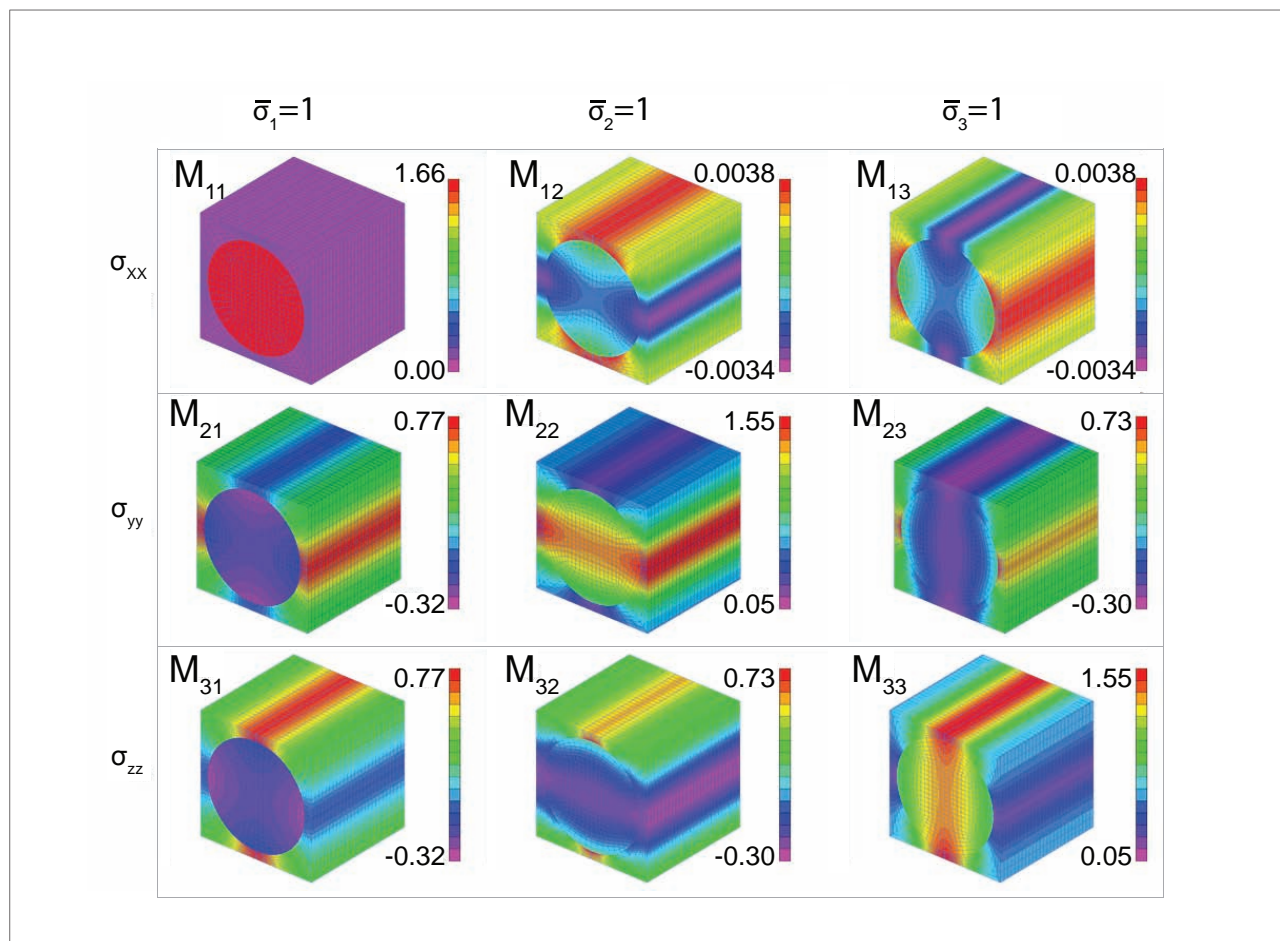Figure 12. Stress contours within the RVE, subjected to macro-mechanical tension load.
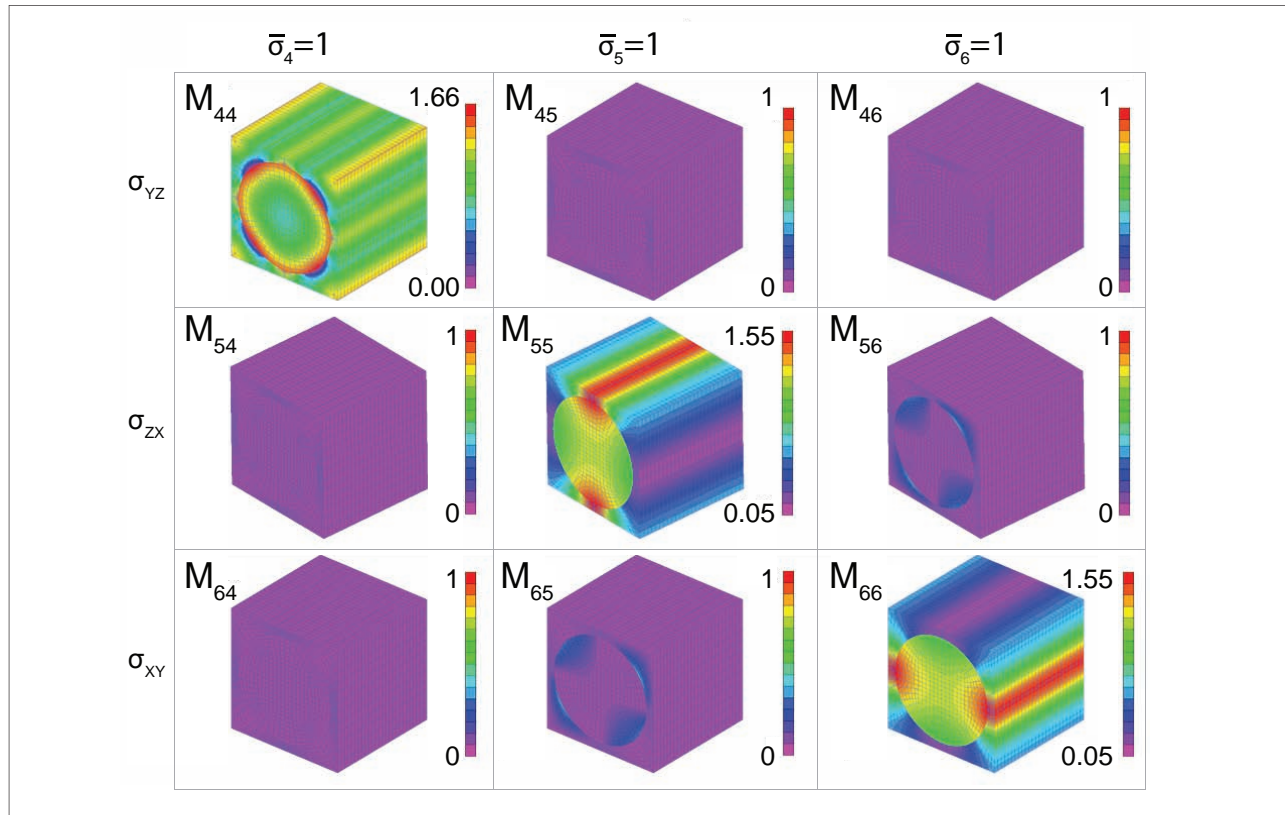
Figure 13. Stress contours within the RVE, subjected to macro-mechanical shear load.

Table 4. Stress amplification factors from Nastran at Point 1, with Mesh 6.

Stress	$\overline{\sigma}_1=1$	$\overline{\sigma}_2=1$	$\overline{\sigma}_3=1$	$\overline{\sigma}_{23}=1$	$\overline{\sigma}_{31}=1$	$\overline{\sigma}_{12}=1$
σ_{xx}	2.43×10^{-2}	7.74×10^{-1}	-8.00×10^{-2}	-1.45×10^{-5}	-2.73×10^{-9}	-2.20×10^{-6}
σ_{yy}	-3.14×10^{-3}	1.50	-2.62×10^{-1}	1.19×10^{-5}	-1.25×10^{-9}	-7.22×10^{-7}
σ_{zz}	2.89×10^{-3}	7.33×10^{-1}	5.14×10^{-2}	-5.32×10^{-5}	-1.32×10^{-9}	-9.73×10^{-7}
σ_{yz}	5.36×10^{-8}	-7.71×10^{-6}	3.59×10^{-6}	1.19	-1.07×10^{-12}	-2.37×10^{-11}
σ_{zx}	-2.38×10^{-10}	1.90×10^{-10}	-1.37×10^{-9}	1.26×10^{-9}	1.60×10^{-1}	-2.67×10^{-5}
σ_{xy}	5.61×10^{-9}	-4.69×10^{-6}	8.96×10^{-7}	-2.94×10^{-9}	-4.85×10^{-6}	1.59

Table 5. Stress amplification factors from SMM at Point 1.

Stress	$\overline{\sigma}_1=1$	$\overline{\sigma}_2=1$	$\overline{\sigma}_3=1$	$\overline{\sigma}_{23}=1$	$\overline{\sigma}_{31}=1$	$\overline{\sigma}_{12}=1$
σ_{xx}	2.43×10^{-2}	7.81×10^{-1}	-8.47×10^{-2}	-1.15×10^{-11}	-1.87×10^{-12}	5.72×10^{-13}
σ_{yy}	-3.22×10^{-3}	1.51	-2.75×10^{-1}	1.95×10^{-11}	2.34×10^{-12}	5.10×10^{-12}
σ_{zz}	2.89×10^{-3}	7.34×10^{-1}	5.06×10^{-2}	-4.29×10^{-11}	5.16×10^{-13}	1.13×10^{-12}
σ_{yz}	1.10×10^{-12}	-5.67×10^{-11}	1.98×10^{-11}	1.21	9.42×10^{-14}	1.15×10^{-13}
σ_{zx}	-4.05×10^{-14}	2.24×10^{-12}	-4.81×10^{-13}	3.63×10^{-12}	1.59×10^{-1}	-2.53×10^{-11}
σ_{xy}	2.27×10^{-15}	-4.80×10^{-13}	3.34×10^{-13}	-1.75×10^{-12}	9.80×10^{-12}	1.59

Table 6. Difference between stress amplification factors between Nastran model (Mesh 6) and SMM at Point 1.

Stress	$\overline{\sigma}_1=1$	$\overline{\sigma}_2=1$	$\overline{\sigma}_3=1$	$\overline{\sigma}_{23}=1$	$\overline{\sigma}_{31}=1$	$\overline{\sigma}_{12}=1$
σ_{xx}	0.00%	0.86%	5.65%	-	-	-
σ_{yy}	2.62%	0.98%	4.82%	-	-	-
σ_{zz}	-0.14%	0.16%	-1.59%	-	-	-
σ_{yz}	-	-	-	1.69%	-	-
σ_{zx}	-	-	-	-	-0.57%	-
σ_{xy}	-	-	-	-	-	-0.15%

Figure 14. Stress contours within the RVE, subjected to thermal load $\Delta T = 1^\circ C$.

Figure 15. Representative volume element in a cutaway view on σ_y stress contour.

reducing the number of elements in x direction. The cubic finite element model showed in Fig. 5 is reduced on its half and the resulting model is called Model 1/2. Those model simplifications are carried out up to Model 1/32, as presented in Fig. 16.

The stress amplification factors found with Models 1 to 1/32 are virtually the same, as long as the mesh stays three-dimensional (solid elements). For example, the difference between the full size model and the one with 1/32 of thickness (Model 1/32) is, in the worst scenario, 0.01%.

The next step of this study is to verify the differences between the results of the three-dimensional Model 1/32 and two-dimensional ones. Two different two-dimensional Nastran elements are used: the four-node (linear) quadrilateral membrane CQUAD4 element and the eight-node (parabolic) quadrilateral membrane CQUAD8.

Figure 17 shows σ_y stress contours for the RVE subjected to a uniformly distributed unit load $\overline{\sigma}_2$. The correspondent stress amplification factors M_{22} are listed in Table 8. Table 9 shows that two-dimensional models fail in calculating accurate in-plane results.

CONCLUSION

In this paper, a finite element procedure is presented to access internal stresses in micromechanical analysis of composites materials, with unidirectional fibers. First, three-dimensional finite element models of a RVE are idealized and modeled in Nastran, with CHEXA (hexahedral), CELAS2 (spring), and rigid (RBE2) elements. Convergence analysis is performed. Stress amplification factors are derived within a RVE under tension, shear, and thermal load. Then, two-dimensional Nastran models are also proposed.

Table 7. Stress amplification factors at Point 1 for thermal load.

Stress	Model	SMM	Difference (%)
σ_{xx}	-1.92×10^5	-1.90×10^5	-0.74
σ_{yy}	2.06×10^5	2.11×10^5	2.59
σ_{zz}	-1.90×10^5	-1.90×10^5	0.17
σ_{yz}	-3.63	-1.75×10^{-5}	$-$
σ_{zx}	-1.02×10^{-5}	7.89×10^{-7}	$-$
σ_{xy}	-5.92×10^{-1}	-1.20×10^7	$-$

Finite element model simplifications

It is notable that all the results are constant within the element along the x axis, as illustrated in details in Fig. 15. This suggests that: a courser three-dimensional mesh can be used at x direction or the model does not need necessarily to be three-dimensional.

A series of model simplifications is carried out. The first part focuses on three-dimensional simplifications by
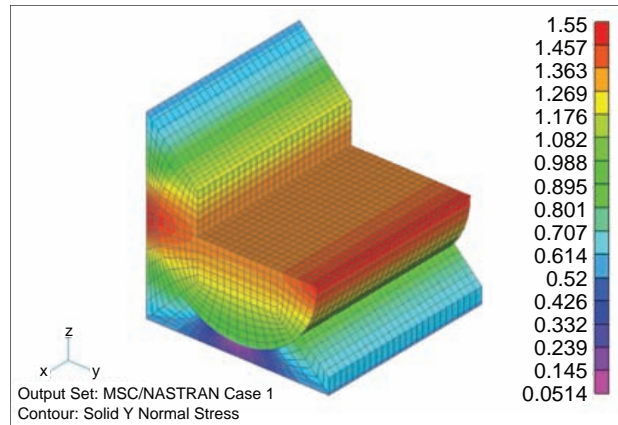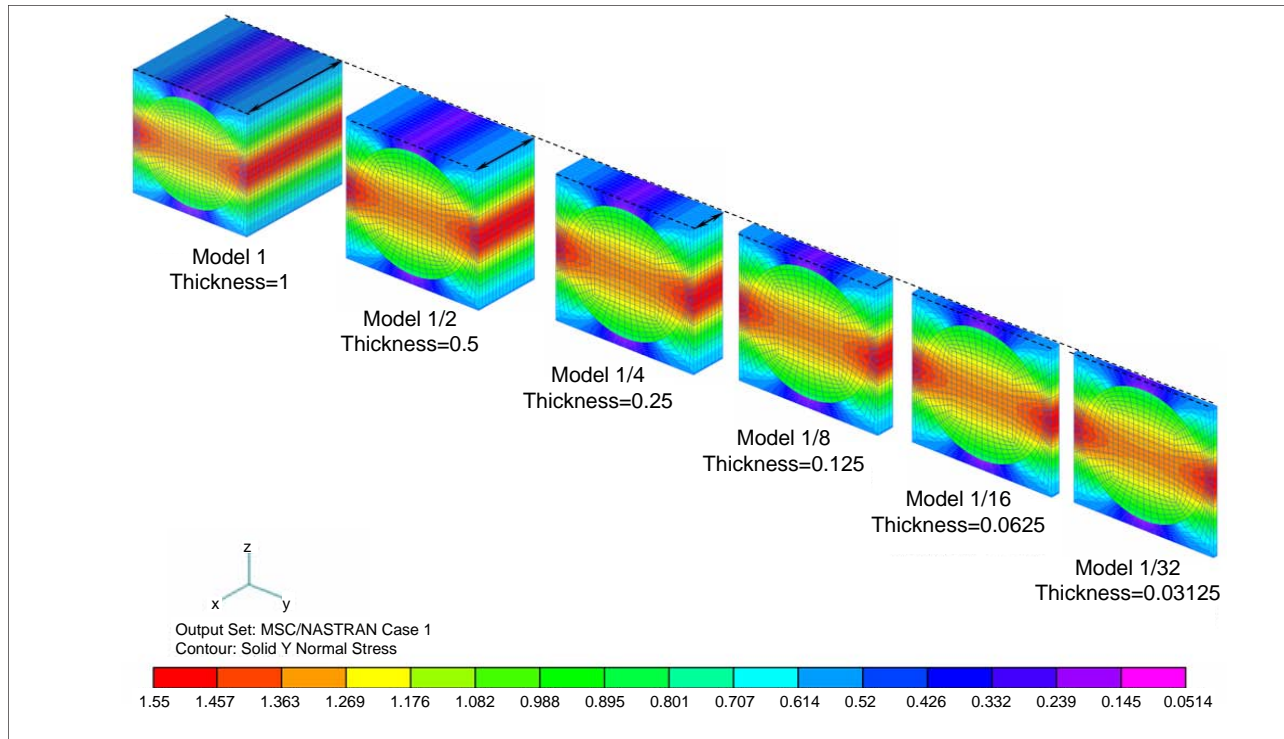
Figure 16. Three-dimensional models for RVE, subjected to macro-mechanical unit load $\overline{\sigma}_2(\sigma_y$ contours).
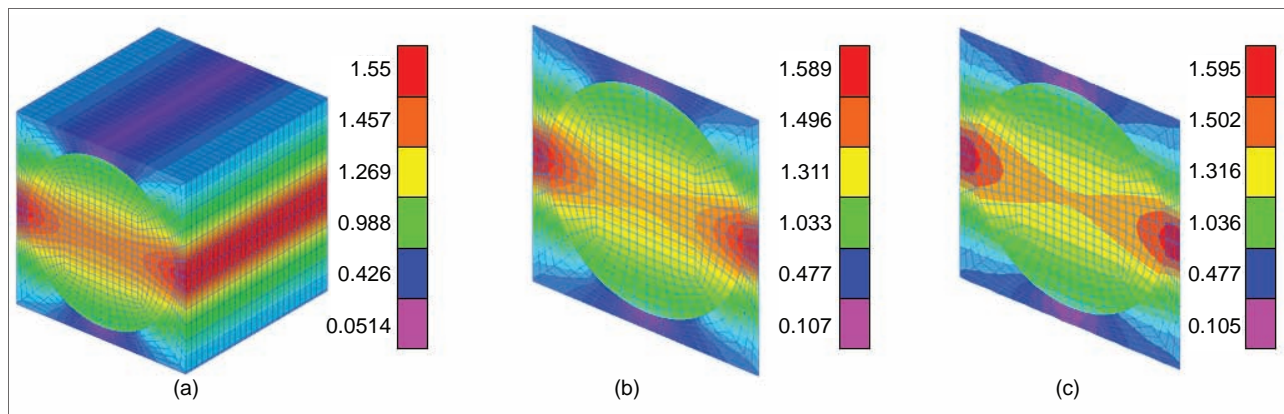

Figure 17. Stress amplification factors M$_{22}$ with: (a) three-dimensional Model 1/32 (2984 DOF); (b) linear membrane elements (1464 DOF); (c) parabolic membrane elements (4368 DOF).

Table 8. Stress amplification factors with parabolic membrane elements.

Stress	$\overline{\sigma}_1=1$	$\overline{\sigma}_2=1$	$\overline{\sigma}_3=1$
σ_{yy}	1.545112	0.152274	-
σ_{zz}	0.480766	0.104816	-
σ_{yz}	-	-	1.287447

Table 9. Differences between stress amplification factors found with Model 1/32 and with parabolic membrane elements.

Stress	$\overline{\sigma}_1=1$	$\overline{\sigma}_2=1$	$\overline{\sigma}_3=1$
σ_{yy}	3.25%	41.92%	-
σ_{zz}	34.38%	103.97%	-
σ_{yz}	-	-	8.17%

The presented two-dimensional models fail in providing accurate in-plane stress amplification factors. Good estimation for internal stress amplification factors is achieved with three-dimensional models. Good results

can be derived with a single transverse layer of solid finite elements, an important feature for nonlinear analyses. The good performance of the presented three-dimensional models shows that good estimates for stress

amplification factors can be derived for other than the presented composite (with another volume fraction, or for bidirectional fibers composite), and also to access strain amplification factors.

REFERENCES

Allix, O., Ladevèze P., Corigliano, A., 1995, "Damage analysis of interlaminar fracture specimens", Composite Structures, Vol. 31, No. 1, p. 61-74. doi:10.1016/0263-8223(95)00002-X

Aghdam, M., Khojeh, A., 2003, "More on the effects of thermal residual and hydrostatic stresses on yelding behavior of unidirectional composites", Composite Structures, Vol. 62., No. 3-4, p. 285-90.

Boeing. 787 Dreamliner – Program Fact Sheet. Retrieved in 2010 August 2, from: http://www.boeing.com/commercial/787family/programfacts.html.

Chaboche, J.L., Kruch, S., Pottier, T., 1998, "Micromechanics versus Macromechanics: a combined approach for metal matrix composites constitutive modeling", European Journal of Mechanics, Vol. 17, No. 6., p. 885-908.

Dragoi, D., et al., 2011, "Investigation of thermal residual stresses in tungsten-fiber/bulk metallic glass matrix composites", Scripta Materialia, Vol. 45, No. 2, p. 245-52.

Fiedler, B., Hojo, M., Ochiai, S., 2002, "The influence of thermal residual stresses on the transverse strength of CRFP using FEM. Composites Part A: Applied Science and Manufacturing", Vol. 33., No. 10, p. 1323-6.

Gotsis, P.K., Chamis, C.C., Minnetyan, L., 1998, "Prediction of Composite laminate fracture: micromechanics and progressive fracture", Composites Science and Technology, Vol. 58, No. 7, p. 1137-49.

Ha, S.K., Huang, Y., Jin, K.K., 2008a, "Effects of Fiber Arrangement on Mechanical Behavior of Unidirectional Composites", Journal of Composites Materials, Vol. 42, No. 18, p. 1851-71.

Ha, S.K., Huang, Y., Jin, K.K., 2008b, "Life Prediction of Composites using MMF and ATM". In: Tsai, S., 2008, "Strength and Life of Composites", Stanford, Department of Aeronautics & Astronautics of Stanford University.

Ha, S.K., Huang, Y., Jin, K.K., 2008c, "Micro-Mechanics of Failure (MMF) for Continuous Fiber Reinforced Composites", Journal of Composites Materials, Vol. 42, No. 18, p. 1873-95.

Hojo, M., et al., 2009, "Effect of fiber array irregularities on microscopic interfacial normal stress states of transversely loaded UD-CFRP from viewpoint of failure initiation", Composites Science and Technology, Vol. 69, No. 11-2, p. 1726-34.

Hyer, M.W., Waas, A.M., 2000, "Micromechanics of Linear Elastic Continuous Fiber Composites", In: Kelly, A., Zweben, C., 2000, "Comprehensive Composite Materials", Elsevier Science Publishers.

Jin, K.K., et al., 2008, "Distribution of micro stresses and interfacial tractions in unidirectional composites", Journal of Composite Materials, Vol. 42, No. 18.

Ladevèze, P., et al., 2005, "Micro and meso computational damage modellings for delamination prediction", ICF XI - 11th International Conference on Fracture.

Liang, Z., Lee, H.K., Suaris, W., 2006, "Micromechanics-based constitutive modeling for unidirectional laminated composites", International Journal of Solids and Structures, Vol. 43, No. 18-9, p. 5674-89.

Msc Software, 2011, "MD Nastran: Integrated, Multidiscipline CAE Solution", Retrieved in 2011 March 23, from http://www.mscsoftware.com/Products/CAE-Tools/MD-Nastran.aspx.

Sagushi, R., Wiltbank, B., Murchison, C., 2004, "Prediction of composite elastic modulus and polymerization shrinkage by computational micromechanics", Dental Materials, Vol. 20, No. 4, p. 397-401.

Sihn, S., Park, J. W., 2008, "An Integrated Design Tool for Failure and Life Prediction of Composites", Journal of Composites Materials, Vol. 42, No. 18, p. 1967-88.

Sun, C. T., Vaidya, R. S., 1996, "Prediction of Composite Properties from a Representative Volume Element", Composites Science and Technology, Vol. 56, No. 2, p. 171-9.

Tay, T.E., et al., 2008, "Progressive Failure Analysis of Composites", Journal of Composites Materials, Vol. 42, No. 18, p. 1921-66.

Taya, M., 1999, "Micromechanics modeling of smart composites. Composites Part A: applied science and manufacturing", Vol. 30, No. 4, p. 531-6.

Think Composites, 2011, "Super Mic-Mac – a new preliminary design tool for composites", Retrieved in 2011 March 23, from http://www.thinkcomposites.com/index_eng.php.

Tsai, S., 2008, "Strength and Life of Composites", 1st ed, Stanford: Department of Aeronautics & Astronautics of Stanford University.

Xia, Z., Zhang, Y., Ellyin, F., 2003, "A unified boundary conditions for representative volume elements of composites and applications", International Journal of Solids and Structures, Vol. 40, No. 8, p. 1907-21.

Zhu, L.J., Cai, W.Z., Tu, S.T., 2009, "Computational Micromechanics of Particle reinforced Composites: Effect of Complex Three-dimensional Microstructures", Journal of Computers, Vol. 4, No. 12, p. 1237-42.